

Diffusion-based Generative AI for Exploring Transition States from 2D Molecular Graphs

Seonghwan Kim^{1†}, Jeheon Woo^{1†} and Woo Youn Kim^{1,2*}

¹Department of Chemistry, KAIST, 291 Daehak-ro, Yuseong-gu, 34141, Daejeon, Republic of Korea.

²AI Institute, KAIST, 291 Daehak-ro, Yuseong-gu, 34141, Daejeon, Republic of Korea.

*Corresponding author(s). E-mail(s): wooyoun@kaist.ac.kr;
Contributing authors: dmdtka00@kaist.ac.kr; woojh@kaist.ac.kr;

[†]These authors contributed equally to this work.

Abstract

The exploration of transition state (TS) geometries is crucial for elucidating chemical reaction mechanisms and modeling their kinetics. Recently, machine learning (ML) models have shown remarkable performance for prediction of TS geometries. However, they require 3D conformations of reactants and products often with their appropriate orientations as input, which demands substantial efforts and computational cost. Here, we propose a generative approach based on the stochastic diffusion method, namely TSDiff, for prediction of TS geometries just from 2D molecular graphs. TSDiff outperformed the existing ML models with 3D geometries in terms of both accuracy and efficiency. Moreover, it enables to sample various TS conformations, because it learned the distribution of TS geometries for diverse reactions in training. Thus, TSDiff was able to find more favorable reaction pathways with lower barrier heights than those in the reference database. These results demonstrate that TSDiff shows promising potential for an efficient and reliable TS exploration.

Keywords: Transition state, Transition state conformation, Chemical reaction, Machine learning, Diffusion model, Generative model

1 Introduction

A transition state (TS) refers to a transient molecular configuration that places on top of the energy barrier that reactants pass through to reach products, corresponding to the saddle point on the minimum energy path between the reactants and products. Identifying TSs is an important task in chemical reaction analysis, such as kinetics modeling [1–6], mechanism studies [7–15], and catalyst design [16–19]. Although TS geometries are difficult to observe experimentally due to their transient nature, they can be obtained using quantum chemical calculation methods. Over the past decades, a variety of TS optimization techniques have been developed and applied to many chemical reactions, thereby providing insights into diverse chemical phenomena [19–27].

TS optimization methods have two primary categories: single-ended [25–27] and double-ended methods [24, 28–35] depending on input types. The former relies on a single set of the 3D geometries of reactants or estimated TSs. One example is the Bernaly algorithm [25] which optimizes a given TS guess geometry to the saddle point of the potential energy surface (PES) using the local surface information of atomic forces and a Hessian. Most single-ended approaches start from the 3D geometries of reactants, such as artificial force-induced reaction (AFIR) [36], anharmonic downward distortion following (ADDF) [37], and single-ended growing string methods (GSMs) [24]. The double-ended methods utilize the 3D geometries of both reactants and products. For example, the nudged elastic band [28–30] and double-ended GSMs [32–34] first search the minimum energy pathway connecting the reactants and products and then identify the maximum energy point on that pathway. While these conventional methods are widely used in practice, they entail large computational cost and often convergence issues, making TS exploration a considerably demanding task.

Recently, there has been a growing interest in using machine learning (ML) methods to investigate the TSs, with the aim of mitigating the high cost of conventional methods. For example, numerous studies have been conducted to directly estimate barrier heights [6, 38–48]. However, we here focus on the prediction of TS geometries [40, 49–53], since it provides atomistic insights into reaction mechanisms and allows the refinement and validation of the predicted TS via post quantum chemical calculations. In the past few years, several ML models have been proposed to accurately predict TS geometries by leveraging the 3D geometries of reactants and products as input, like the double-ended methods [40, 49–53]. The validity of these models was demonstrated with density functional theory (DFT) calculations. They have exhibited promising results on a general gas-phase reaction database [54] as well as specific reaction categories, such as S_N2 and hydrogen transfer reactions, indicating their potential to complement expensive quantum chemical calculations. Despite their remarkable achievements, it should be noted that they still require well-aligned reactant and product geometries along the reaction coordinates.

Both the conventional and ML approaches need an appropriate input preparation for 3D molecular geometries. However, it is well known that the

results of the conventional approaches are sensitive to the input structures [33, 34, 55, 56]. The ML approaches also take the 3D conformations of reactants and products as input. Thus, it is inevitable for them to share the same input sensitivity issue. As pointed out by numerous studies, ML models using 3D molecular geometries as input are known to be input sensitive across various fields [39, 57, 58]. In the TS prediction task, Choi [52] shows that perturbations to the input geometries can result in a different TS geometry. Therefore, in practical applications, the input preparation becomes an important procedure affecting the quality of prediction results. To obtain an appropriate input, the molecular orientation should be considered along the target reaction coordinates, which requires careful consideration even by professional chemists. Moreover, it is necessary to explore possible TS conformations to elucidate the most favorable reaction pathway [59–62], which makes the preparation task more demanding to cope with various conformations.

To address this problem, we present TSDiff, an ML model that learns a direct mapping between TS conformations and 2D molecular graphs. Thus, one can skip the proper selection of conformations and orientations. Moreover, TSDiff can generate various TS conformations possible from the 2D graph, with high reliability by employing the stochastic diffusion method which has been used to generate molecular conformers in equilibrium [63–65]. Consequently, TSDiff can minimize user efforts throughout the entire TS generation process and explore multiple reaction pathways without the direct consideration of conformations, leading to high efficiency.

In this study, the performance of TSDiff was evaluated using a general organic gas-phase reaction database [54]. Despite its simplified input of 2D graphs, TSDiff has achieved comparable accuracy to the existing methods that rely on 3D geometric information. The validity of multiple TS conformations generated by TSDiff was verified quantum chemically using saddle point optimization [25] and subsequent intrinsic reaction coordinate (IRC) [66] calculations. TSDiff achieved significantly high success rates of 97.4 % and 90.6 % in the two calculations, respectively, showing its reliability as an initial TS geometry guesser. We also found 2,303 new TS conformations at saddle points other than the reference using TSDiff with eight rounds of sampling. Some of these corresponded to lower barrier heights than those of the references, suggesting more favorable reaction pathways. It is worth noting that TSDiff was trained with only one TS conformation for each reaction, underscoring its outstanding generative performance in this context. Overall, our findings demonstrate the potential of TSDiff as a new promising approach for efficient and reliable TS exploration.

2 Results

2.1 A brief description of the generation process

In this section, we provide a brief overview of TSDiff, an ML model designed to learn the conditional distribution of 3D TS geometries given 2D reaction

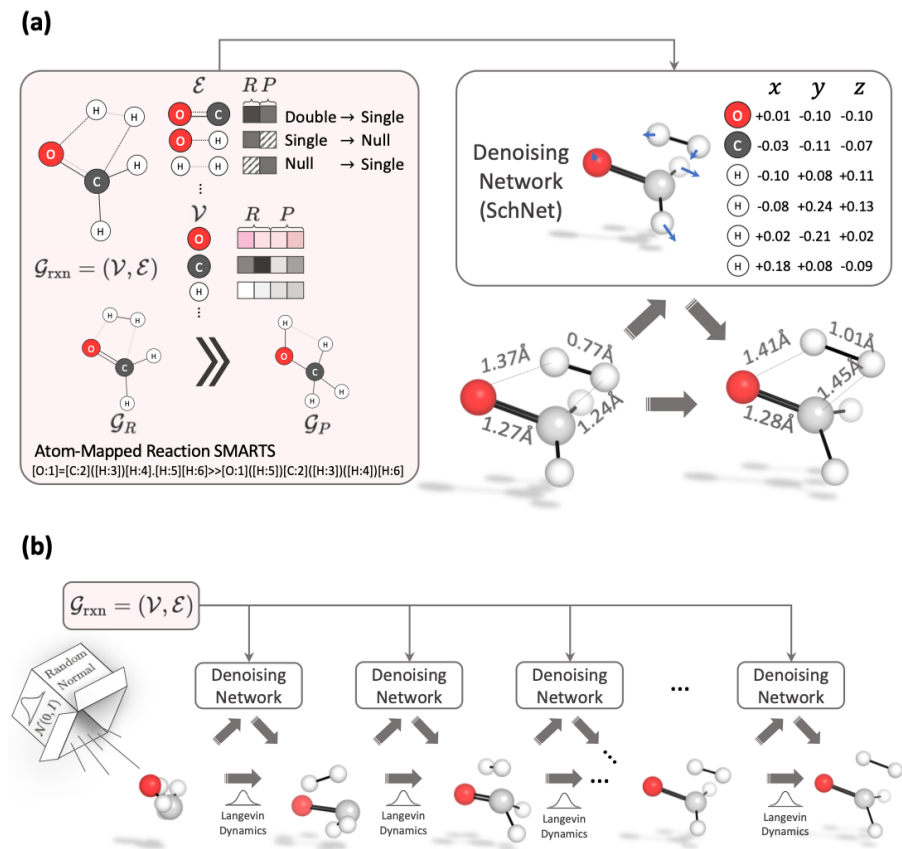


Fig. 1 Overview of the proposed TSDiff. **a** Illustration of the reaction graph and the denoising network. The denoising network denoises a given geometry input based on the reaction graph constructed by combining the molecular graphs of the reactant and product. **b** Transition state (TS) generation procedure of the proposed TSDiff via Langevin dynamics. Starting from a randomly initialized geometry, the geometry is progressively refined by the denoising network until reaching a predicted TS geometry. All molecular geometries were plotted using PyMOL [67].

information presented as SMARTS [68] (see Fig. 1a). TSDiff is based on the stochastic denoising diffusion method, which trains the model to learn the reverse process of a hyperparameterized noise process that adds random noise to the given geometry at each discrete time step. At the inference phase, the model generates TS geometries from the noise sampled from a predefined random distribution. The process is an iterative denoising process that utilizes Langevin dynamics [69], which is illustrated in Fig. 1b. The noisy input is stochastically denoised at each time step given the 2D reaction information.

The input of the model is 2D reaction information expressed as a reaction graph \mathcal{G}_{rxn} which captures the bond changes in reactants and products [70]. The simplified version of the reaction graph is depicted in the left box of Fig. 1a.

Molecular graphs for reactants and products, \mathcal{G}_R and \mathcal{G}_P , can be constructed based on bond and atom information that can be obtained from SMILES [71]. The nodes in the graph are represented as atom-feature vectors containing atomic numbers. For the edges, the molecular graphs utilize extended graph edges that include node-pair indices within a 3-hop graph distance in the raw graph created based on covalent bonds. The condensed reaction graph, which serves as our model input, is formed by combining the two graphs of reactants and products using atom-mapping information.

TSDiff employs graph neural network (GNN) layers based on SchNet [72] to handle the noised positions and reaction graphs. A geometric reaction graph is created by adding the noised positions to the 2D reaction graph and connecting nodes with interatomic distances smaller than a predefined cutoff. Thus, the geometric graph includes bond information, graph distance information, and spatial distance information as edge-features. The model then predicts changes in atomic positions using the geometric graphs. More details are described in the “TSDiff” section.

The proposed TSDiff was trained and validated using the general organic gas-phase reaction database published by Grambow et al [54]. We employed an ensemble with a total of eight models, and our training process took 22 hours for each model on a single RTX 2080 Ti NVIDIA GPU. For most results reported in the following sections, we used the ensemble model and will refer to it as TSDiff unless otherwise noted.

2.2 Generation of TS conformations

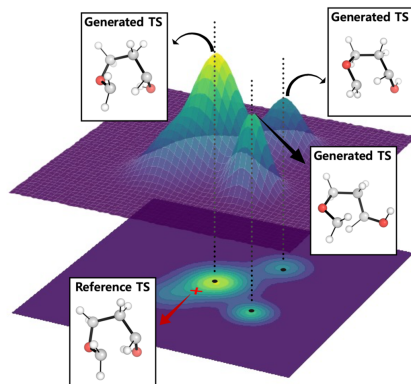


Fig. 2 Conceptual illustration of predictive distribution of TSDiff. The 3D surface represents a probability distribution of predicted TS geometries. Examples of reference and generated transition state (TS) geometries are visualized in the boxes. The generated geometries extracted from each peak have different conformations from each other. All molecular geometries were plotted using PyMOL [67].

We emphasize that TSDiff is a stochastic generative model, implying that different geometries are generated at each sampling. Figure 2 depicts a conceptual representation of TSDiff’s predictive distribution. The different geometries generated by TSDiff correspond to specific conformations that can be built from the same 2D reaction graph. For example, Fig. 3 shows several generated geometries corresponding to specific conformations and reference geometries for three reactions in the test set. This is an inherent outcome because TSDiff uses only 2D graphs as input. Also, the reference TS would be one of various TS conformations identified by a specific computational method. Therefore, it is essential to consider diverse conformations and the comparative analysis of their barrier heights in the TS exploration process in order to identify the most favorable reaction pathway. Thanks to the nature of generative AI, TSDiff learns the distribution of TS geometries for diverse reactions in training, facilitating the reliable sampling of these different TS conformations.

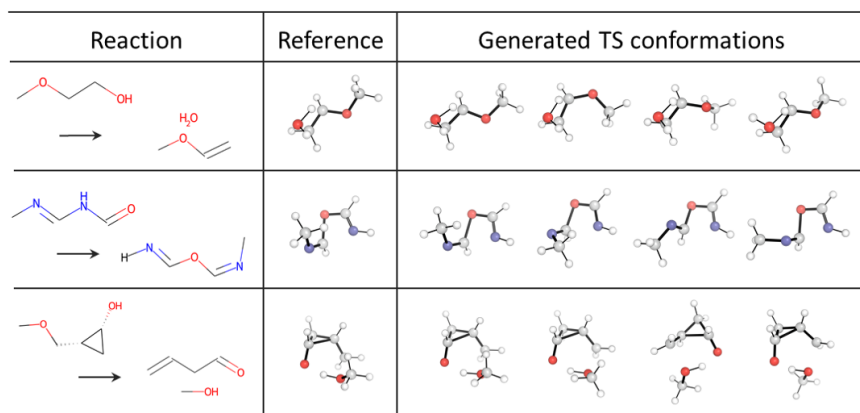


Fig. 3 Examples of transition state (TS) conformations generated by TSDiff. For each reaction, we sampled multiple TS geometries and picked four different conformations including one that was best-aligned with the reference one. All molecular geometries were plotted using PyMOL [67].

The various conformations generated by TSDiff need to be verified to ensure that they are indeed chemically valid TSs. As an example, we performed quantum chemical validation on a single test reaction. First, TSDiff generated one hundred samples for this reaction, which were then optimized using a saddle point optimization. Figure 4 visualizes the distribution of the generated geometries using t-SNE [73] in scikit-learn [74]. Each dot in the figure represents a generated geometry, while the star and cross-shaped dots indicate the optimized and reference geometries, respectively. Additionally, each dot has been color-coded to reflect its respective optimization result. For example, all generated geometries represented by the blue dots were optimized to the geometry represented by the blue star-shaped dot via the saddle point optimization.

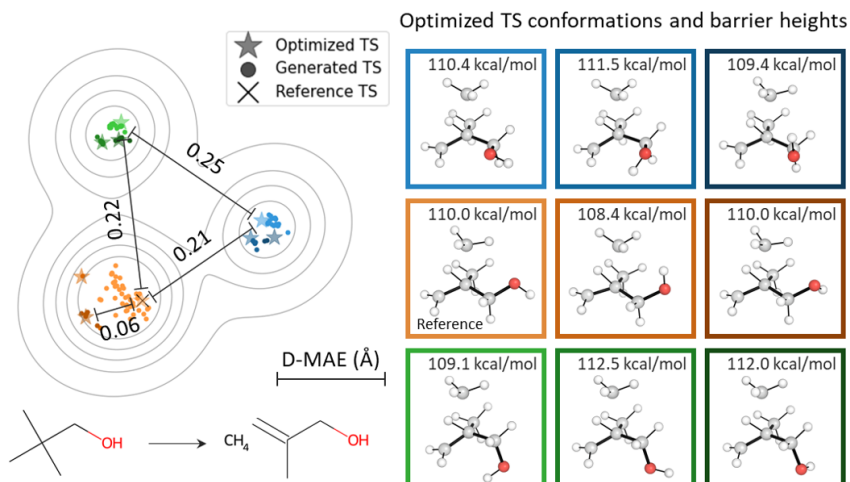


Fig. 4 Visualization of the geometries generated by TSDiff. The dots in the left side image denote the geometries generated by TSDiff for the given reaction below. To visualize the distribution, the t-SNE method was used with the interatomic distances of the geometries as input. The images on the right side show nine different optimized TS conformations and their barrier heights. All molecular geometries were plotted using PyMOL [67].

All one hundred generated geometries were successfully optimized to saddle points, resulting in nine different TS conformations. The images on the right side of Fig. 4 show the optimized conformations. The different conformations were caused by two rotatable single bonds closest to oxygen, “C–C” and “C–O”. There were three major conformational changes with different dihedral angles centered on the “C–C” bond, and for each there were three minor conformations with different dihedral angles centered on the “C–O” bond, resulting in a total of nine different conformations. Here, the accuracy of the generated geometries was measured by the mean absolute error (MAE) of interatomic distances, D–MAE, with respect to their corresponding optimized results. A detailed method for measuring the D–MAE is given in “Measurement details”. The resulting average D–MAE was very small at 0.045 Å, indicating that the generated samples were optimized to the respective saddle points with only minor adjustments.

The resulting optimized geometries were confirmed as valid TS geometries using IRC calculations. A detailed description of the IRC and validation method is provided in the “Computational details”. This result indicates that TSDiff can find not only a conformation that corresponds to the reference geometry but also other valid TS conformations. Interestingly, the discovered TS conformations include TSs with lower barrier heights than that of the reference, as shown in Fig. 4. This proves that the reference TS may not be the most favorable one, even though it was built using the most stable molecular conformation of the reactants [54], highlighting the importance of exploring

multiple TS conformations. As a result, we demonstrate that the stochastic diffusion model, which has already shown its capability of accurately generating conformers in equilibrium, can be extended to TS explorations.

2.3 Performance of TS generation

From the perspective of a generative AI, it is important to evaluate the ability of TSDiff to generate samples that cover the reference TS of the dataset and how accurate the generated samples are. To this end, we calculated the following two metrics for all reactions in the test set: coverage (COV) and matching (MAT) scores. The COV score measures the percentage of the reference TS geometries covered by the predicted ones by TSDiff, where a reference is considered to be covered if there exists any predicted one having a D-MAE of 0.1 Å or less with the reference. This criterion of 0.1 Å was determined based on the accuracy of a state-of-the-art model [52] which has demonstrated reliability with a high success rate in quantum chemical validations. The MAT score measures the similarity between generated and reference samples by calculating the minimum D-MAE between the generated geometries and the reference geometry. The mathematical definitions of these two metrics can be found in the “Measurement details”.

Table 1 The coverage (COV) and matching (MAT) scores of TSDiff according to the number of sampling. The results of two TSDiff models with and without the ensemble method are compared.

# of sampling	ensemble		no ensemble	
	COV (%) ↑	MAT (Å) ↓	COV (%) ↑	MAT (Å) ↓
1	49.1	0.137	47.7	0.141
3	67.3	0.096	65.7	0.100
5	75.2	0.079	74.0	0.085
10	83.9	0.064	80.2	0.072
100	91.7	0.046	89.6	0.053

While these two metrics are widely used for generative AI evaluation, it should be noted that they have a limited application in this study because there is only one TS conformation for each reaction in the reference dataset. Therefore, for each individual reaction, the COV score is either 100 % or 0 % if only a single sample is used for evaluation. Moreover, the COV and MAT scores may be underestimated when the number of sampling is small, given that TSDiff generates various conformations. Thus, Table 1 presents the COV and MAT scores of TSDiff according to the number of sampling, including a comparison to the scores of TSDiff without the ensemble method. The distributions of the MAT scores across the reaction are shown in Fig. 5.

The COV and MAT scores are improved rapidly as the number of sampling increases. This is because TSDiff’s performance is underestimated at small numbers of the sampling, as it generates many different conformations, as shown in Fig. 3. In addition, the ensemble method led to slight performance improvements in both COV and MAT scores. As a result, TSDiff is expected

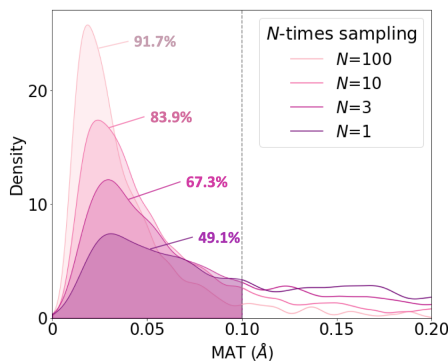


Fig. 5 The distribution of the matching (MAT) scores of TSDiff with the number of sampling. The percentages represent the coverage (COV) scores measured using the D-MAE threshold of 0.1 Å.

to be able to generate 83.9 % of the reference TSs with a D-MAE of 0.1 Å or less within ten rounds of sampling.

Table 2 Comparison of accuracies and features between machine learning models. The input type, target type, and accuracy of the models are compared. Accuracy is measured using the mean absolute error of interatomic distances (D-MAE) for existing models and the matching (MAT) score for TSDiff as a generative model. C_R and C_P denote the geometries of reactants and products, respectively, and \mathcal{G}_R and \mathcal{G}_P denote the 2D graphs of reactants and products, respectively. $(C_R+C_P)/2$ denotes the interpolated geometry between C_R and C_P .

model	input type	target type	D-MAE / MAT (Å)
Makoš et al. [50]	C_R, C_P	CM ¹	0.170 / -
Jackson et al. [49]	C_R, C_P	positions	0.244 ² / -
Pattanaik et al. [51]	$C_R, C_P, \mathcal{G}_R, \mathcal{G}_P$	distances	0.225 ² / -
Choi [52]	$C_R, C_P, (C_R+C_P)/2$	distances	0.095 ² / -
TSDiff	$\mathcal{G}_R, \mathcal{G}_P$	positions	- / 0.137, 0.079, 0.063 ³

¹CM indicates the Coulomb matrix.

²The values are borrowed from Choi [52].

³The three values are the MAT scores when the number of sampling is 1, 5, and 10, respectively.

We compare the features and accuracies of TSDiff and the existing ML models in Table 2. To the best of our knowledge, Table 2 includes all the models whose performance has been reported on the Grambow’s dataset [54]. Previous works commonly used geometries of reactants and products for their input features [49–52], and the most recently reported model by Choi additionally used the interpolated geometries of reactants and products [52]. Their prediction targets are broadly divided into two categories: interatomic distances and atomic positions. The models that predict interatomic distances require an additional step of a nonlinear least-squares optimization to restore

the distances to atomic positions. In contrast, Jackson et al. directly predicted atomic positions using tensor field networks [49].

TSDiff also targets atomic positions directly in its generation process. A unique feature that distinguishes it from the existing models is that TSDiff uses only 2D graphs as input. Nevertheless, TSDiff could generate highly accurate TS geometries. Table 2 shows the accuracy of the existing models with D-MAEs, while the accuracy of TSDiff is presented using the MAT metric. It is worth noting that since TSDiff was evaluated as a generative AI, it is difficult to compare its performance under the same condition with the existing models. However, based on TSDiff's high COV and low MAT scores, it can be inferred that TSDiff generates TS geometries with an accuracy comparable to or better than the existing models, even without computationally expensive 3D geometric information.

2.4 Quantum chemical validation of generated conformations

As an extension of the experiment in Fig. 4, we evaluate the chemical validity of TS conformations generated by TSDiff across reactions in the test set. We performed TS optimizations based on DFT using the generated geometries for 1,197 reactions in the test set. Eight geometries were generated for each reaction, and saddle point optimization was performed on the resulting 9,576 geometries. Of these, 9,289 were successfully optimized with a single imaginary vibrational frequency, giving a high success rate of about 97.0 %. To determine how various TS conformations were found by TSDiff, we counted the number of differently optimized results. The optimized geometries were distinguished if the D-MAE between them was greater than 0.01 Å. As a result, we confirmed that 3,316 unique TS conformations were obtained, of which 2,303 samples corresponded to different saddle points than those of the reference TSs.

In Table 1, the accuracy of the generated geometries could only be evaluated by the MAT score because multiple conformations were generated, while there was only one conformation for each reaction in the reference dataset. Here, however, their accuracy can be evaluated using their corresponding optimized geometries as a reference. We calculated the D-MAE between the generated geometry and its optimized result for the 9,289 samples succeeded in the saddle point optimization. This resulted in an average D-MAE of 0.083 Å. This number may be slightly underestimated because it does not include the D-MAEs of the samples that failed the optimization, which could be interpreted as outliers. Nevertheless, the high success rate of the saddle point optimization and the small D-MAE of 0.083 Å clearly demonstrate the reliability of TSDiff as an efficient initial TS guesser.

To evaluate the barrier heights of the pathways through the newly discovered TS geometries, we first carried out an IRC validation on them. Due to the huge computational cost, the IRC calculations were performed on one randomly selected geometry for each reaction, where samples that failed the saddle point optimization were considered as failures without IRC validation.

For 998 reactions, corresponding to 83.4 % of the test set, the IRC calculations successfully converged by linking the saddle point to the correct reactants and products. Their barrier heights were calculated with the energy difference between the optimized TS and the reference reactants. Consequently, we found 309 new pathways with barrier heights that were at least 0.1 kcal/mol lower than those of the references.

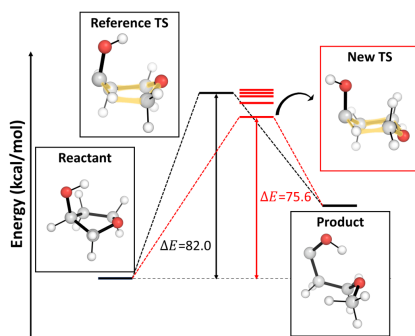


Fig. 6 Comparison of the barrier heights of the reference and those found by TSDiff. The TS conformations were obtained by saddle point optimization using the initial geometries generated by TSDiff, and their energy levels are shown as red lines. The geometries of the reference database are visualized in the black boxes, and the newly discovered TS conformation with the lowest energy is visualized in the red box. All molecular geometries were plotted using PyMOL [67].

Figure 6 shows an example case where TSDiff found TS conformations with lower energies than that of the reference. Five different TS conformations were obtained by saddle point optimization, and their energy levels are indicated by the red lines. The lowest energy conformation in the red box has an energy 6.4 kcal/mol lower than that of the reference, suggesting a more favorable reaction pathway. This substantial energy difference between the reference and the new TS conformations is due to the apparent geometric difference between them, where the hexagonal rings, highlighted in yellow, have the boat and chair conformations in the reference and the new TS, respectively. This emphasizes the importance of searching for different TS conformations to find a more favorable reaction pathway, and TSDiff can be used for this purpose.

2.5 Analysis on failure cases

To further assess the coverage ability of TSDiff based on DFT calculations, we analyzed 199 reactions where the model failed to generate the correct TS within a single sampling. We performed up to four additional random samplings and validated the generated samples using the same process as in the previous section. This resulted in the identification of 89 correct TS geometries among 199. Of the remaining 110 reactions still not covered by TSDiff, we found that several samples were successfully optimized to their reference geometries but

failed the IRC validation. We note that the IRC calculation of the reference TS may fail due to the lack of an IRC verification step during the data generation process [52, 54].

Considering this point, we conducted IRC calculations on the reference TSs of the 110 reactions to confirm whether or not they are elementary step reactions. Among them, 95 reference TSs failed the IRC calculation, which highlights requirements of re-evaluating TSDiff’s performance on the remaining 1,102 reactions after excluding them. Then, TSDiff achieved a success rate of 97.4 %, with 8,588 of the 8,816 samples successfully optimized to the saddle point, as described in Table 3. The success rate of IRC validation for geometries generated by the single sampling was also recalculated to 90.6 %, which was reported as 83.4 % in the previous section. Finally, 98.6% of the refined test reactions were successfully covered by TSDiff within five rounds of sampling, which resulted in the correct TSs on 1,087 reactions.

Table 3 Success rates of quantum chemical validations on geometries generated by TSDiff. For a total of 1,197 reactions, the saddle point optimization was performed on the TS geometries generated with eight rounds of sampling, while the IRC calculation was performed on one randomly selected geometry for each reaction. We found 95 invalid reactions in the original test set for which the reference TS failed the IRC validation. Therefore, the success rates of the quantum chemical calculations were recalculated with the refined 1,102 reactions, after excluding the failed ones.

test reaction	# of reactions	saddle point	IRC
original	1,197	97.0 %	83.4 %
refined	1,102	97.4 %	90.6 %
refined	1,102	99.9 % ¹	98.6 % ¹

¹The value is the cumulative success rate over five rounds of sampling.

3 Discussion

This study has introduced TSDiff, a machine learning (ML) model for exploring transition state (TS) geometries. TSDiff overcomes the limitations of previous ML models, which required the 3D geometries of reactants and products, by generating TS geometries only from 2D molecular graphs. Moreover, TSDiff achieved high accuracy comparable to the existing models based on 3D information. Although TSDiff learned only one TS conformation for each reaction during the training phase, it was able to generate various TS geometries by employing a stochastic diffusion method. The validity of various TS conformations generated by TSDiff was proven through quantum chemical calculations. They were successful in optimization with a high rate, proving the practicality of TSDiff as a reliable initial TS guesser. Furthermore, it generated many valid TS conformations not included in the reference data. Some of these had lower barrier heights than those of the reference TSs, suggesting more favorable reaction pathways and emphasizing the importance of exploring diverse

TS conformations. These findings show that the stochastic diffusion method proven to accurately create diverse conformers in equilibrium states can be extended to TS explorations. It should be noted that the evaluation of TSDiff as a generative AI was limited by the reference dataset with only one TS conformation for each reaction. Nonetheless, this study shows the promising potential of TSDiff for efficient and reliable TS exploration.

4 Methods

4.1 TSDiff

The diffusion process is a stochastic process where atomic positions change into chaotic states at discrete time steps. For a reference TS geometry \mathcal{C}_0 and a geometry at time step t of the diffusive process \mathcal{C}_t , we define the probability distribution q of the diffusive process as follows:

$$\begin{aligned} q(\mathcal{C}_t|\mathcal{C}_{t-1}) &= \mathcal{N}(\mathcal{C}_t; \sqrt{\alpha_t}\mathcal{C}_{t-1}, \beta_t I), \\ q(\mathcal{C}_t|\mathcal{C}_0) &= \mathcal{N}(\mathcal{C}_t; \sqrt{\bar{\alpha}_t}\mathcal{C}_0, (1 - \bar{\alpha}_t)I). \end{aligned} \quad (1)$$

Here, the hyperparameters β_t and $\alpha_t (= 1 - \beta_t)$ denote the noise and signal schedulers, respectively, which determine how much noise to add and how much of the existing signal to preserve at time step t , and $\bar{\alpha}_t = \prod_{s=1}^t \alpha_s$. The neural network model learns a distribution parameterized by θ , p_θ , that simulates the reverse process of the diffusion process:

$$p_\theta(\mathcal{C}_{t-1}|\mathcal{C}_t, \mathcal{G}_{\text{rxn}}) = \mathcal{N}\left(\mathcal{C}_{t-1}; \mu_\theta(\mathcal{C}_t, \mathcal{G}_{\text{rxn}}, t), \sigma_t^2 I\right), \quad (2)$$

where \mathcal{G}_{rxn} denotes the input reaction graph, and μ_θ and σ_t^2 denote the mean and the variance of the distribution, respectively. The loss form is defined as the KL divergence between the posterior of q and p_θ at each time step $t \leq T$:

$$\begin{aligned} \log p_\theta(\mathcal{C}_0|\mathcal{G}) &\geq - \sum_{t=1}^T \text{KL}(q(\mathcal{C}_{t-1}|\mathcal{C}_t, \mathcal{C}_0) \| p_\theta(\mathcal{C}_{t-1}|\mathcal{C}_t, \mathcal{G}_{\text{rxn}})) \\ &\quad - \text{KL}(q(\mathcal{C}_T|\mathcal{C}_0) \| p_\theta(\mathcal{C}_T)) \\ &\quad + \mathbb{E}_{q(\mathcal{C}_1|\mathcal{C}_0)} [\log p_\theta(\mathcal{C}_0|\mathcal{C}_1, \mathcal{G}_{\text{rxn}})], \end{aligned} \quad (3)$$

where $p_\theta(\mathcal{C}_T)$ is a unit Gaussian prior. Minimizing the KL divergence of Eq. (3) implicitly maximizes $\log p_\theta(\mathcal{C}_0|\mathcal{G}_{\text{rxn}})$ which is the main objective of the reference TS generation.

From the Gaussian distribution assumption of p_θ and q , the KL term is derived to the simple form as:

$$\text{KL} (q(\mathcal{C}_{t-1}|\mathcal{C}_t, \mathcal{C}_0) \| p_\theta(\mathcal{C}_{t-1}|\mathcal{C}_t, \mathcal{G}_{\text{rxn}})) = \mathbb{E}_q \left[\frac{\beta_t^2}{2\alpha_t(1-\bar{\alpha}_t)\sigma_t^2} \|\epsilon - \epsilon_\theta(\mathcal{C}_t, \mathcal{G}_{\text{rxn}}, t)\|_2^2 \right], \quad (4)$$

where $\epsilon = \frac{\mathcal{C}_t - \sqrt{\bar{\alpha}_t}\mathcal{C}_0}{\sqrt{1-\bar{\alpha}_t}} = \sqrt{1-\bar{\alpha}_t}\nabla_{\mathcal{C}_t} \log q(\mathcal{C}_t|\mathcal{C}_0)$ and $\epsilon_\theta = \frac{\sqrt{1-\bar{\alpha}_t}}{\beta_t} (\mathcal{C}_t - \sqrt{\bar{\alpha}_t}\mu_\theta)$ [75]. The tractable loss form of Eq. (4), $\|\epsilon - \epsilon_\theta\|_2^2$, can be interpreted as the score matching loss [63, 76, 77]. To satisfy SE(3) equivariance, which is necessary for the two conditional distributions p_θ and q , we change the score function of the distribution of atomic positions to the score function of pairwise distances using the chain rule. Our diffusive process design is based on Xu et al. [63], so a more detailed description of the diffusion process can be found in the paper. We set the max time step T to 5,000 and used a sigmoid scheduler for β_t .

TSDiff employed a total of seven modified SchNet layers. A geometric reaction graph is created by adding the noised positions to the 2D reaction graph, and it is fed to the GNN layers. The node-vector update step is a conventional message-passing process defined as

$$h_i^{l+1} = \text{MLP}_1^l \left(\text{MLP}_2^l(h_i^l) + \sum_{j \in \mathcal{N}(i)} m_{ij}^l \right), \quad (5)$$

where h_i^l denotes the i -th node-vector at the l -th layer, and m_{ij}^l denotes the message from the j -th node connected to the i -th node. The message is constructed using both atom-pair distances \mathbf{d}_{ij} and edge-features f_{ij}^{rxn} :

$$m_{ij}^l = \text{MLP}_2^l(h_j^l) \left(\pi_{\text{rbf}}^l(\mathbf{d}_{ij}) \odot \pi_{\text{edge}}(f_{ij}^{\text{rxn}}) \right), \quad (6)$$

where π_{rbf}^l and π_{edge} denote a radial basis kernel and an edge-feature embedding function, respectively, and \odot denotes element-wise multiplication. A node-embedding function π_{node} is used to generate the initial node-vector h_i^1 by processing a node-feature vector of the reaction graph f_i^{rxn} . The node-features and edge-features of the reaction graph are first constructed by concatenating those of \mathcal{G}_R and \mathcal{G}_P , respectively: $f_i^{\text{rxn}} = f_i^R \oplus f_i^P$ and $f_{ij}^{\text{rxn}} = f_{ij}^R \oplus f_{ij}^P$. The edge-features contain bond-type information, and the node-features contain various atomic information, such as aromaticity, formal-charge, hybridization, valency, chirality, and whether the atom is in a ring. When an edge does not exist on one side of \mathcal{G}_R or \mathcal{G}_P , the edge-feature of the molecular graph is adjusted with a zero feature vector. To utilize the reaction graph more informatively, we extended \mathcal{G}_R and \mathcal{G}_P to include edges within the 3-hop and encoded their edge-features based on the graph-distances. Additionally, we added edges between nodes within 10.0 Å of the pairwise distances and assigned zero vectors as edge-features.

The neural network predicts \mathcal{C}_{t-1} based on the diffusive geometry \mathcal{C}_t and the reaction graph \mathcal{G}_{rxn} as input by capturing the changes in atomic positions ϵ_θ . Technically, it first calculates the changes in the node-pair distances using the outcomes of L layers of GNN, $\partial \mathbf{d}_{ij} = \psi(h_i^L, h_j^L, f_{ij}^{\text{rxn}}, \mathbf{d}_{ij})$, and they are converted to the changes in atomic positions using a chain rule. In the inference step, the learned reverse dynamics are applied to the randomly sampled noise \mathcal{C}_T from $p(\mathcal{C}_T) \sim \mathcal{N}(0, I)$. The Langevin dynamics is employed for the iterative sampling of \mathcal{C}_{t-1} from the parameterized distribution $p_\theta(\mathcal{C}_{t-1}|\mathcal{C}_t, \mathcal{G}_{\text{rxn}})$, resulting in \mathcal{C}_0 . This overall process could be interpreted as a Markov chain that gradually converges the noised geometry to the reference geometry.

4.2 Data

In this study, we used a publicly available chemical reaction dataset provided by Grambow et al [54]. This consists of gas-phase reactions involving GDB-7 [78] molecules. The reaction pathways were first elucidated using DFT calculations, specifically the single-ended growing string method, and the TS geometries were computed using the saddle point optimization at the same level of theory. There are two types of datasets calculated by different DFT methods, namely B97-D3/def2-mSVP and ω B97X-D3/def2-TZVP, and we used the ω B97X-D3 dataset. Out of the 11,961 reactions in the ω B97X-D3 dataset, we excluded two that involved non-reactive molecular nitrogen. Since our model only captures reaction information with 2D graphs, including these non-reactive molecules could lead to erroneous graph-embedding. We used a total of 11,959 reactions and randomly split the dataset in a ratio of 8:1:1. To improve the performance of our model, we also augmented our training data by including reverse reactions, i.e., swapping the reactants and products, resulting in a total of 19,132 training data points.

4.3 Measurement details

To measure the accuracy of the generated TS geometries, we used the D-MAE metric, which is the MAE of the interatomic distances. The D-MAE between two different geometries, \mathcal{C} and $\hat{\mathcal{C}}$, is defined as

$$\text{D-MAE}(\mathcal{C}, \hat{\mathcal{C}}) = \frac{2}{N_{\text{atom}}(N_{\text{atom}} - 1)} \sum_{i < j}^{N_{\text{atom}}} \left| \mathbf{d}_{ij} - \hat{\mathbf{d}}_{ij} \right|, \quad (7)$$

where \mathbf{d}_{ij} and $\hat{\mathbf{d}}_{ij}$ denote the interatomic distances between the i -th and j -th atoms of \mathcal{C} and $\hat{\mathcal{C}}$, respectively, and N_{atom} is the number of atoms. We performed an atom index alignment between \mathcal{C} and $\hat{\mathcal{C}}$ to minimize the D-MAE between them. This is necessary to match the indices of nodes that are indistinguishable on the molecular graph, such as hydrogen in a methyl group.

To evaluate TSDiff from the perspective of a generative model, we used the COV and MAT scores. The two scores are defined as

$$\text{COV}(S_{\text{gen}}, S_{\text{ref}}) = \frac{1}{|S_{\text{ref}}|} \left| \left\{ \mathcal{C} \in S_{\text{ref}} \mid \text{D-MAE}(\mathcal{C}, \hat{\mathcal{C}}) < 0.1 \text{ \AA}, \hat{\mathcal{C}} \in S_{\text{gen}} \right\} \right|, \quad (8)$$

$$\text{MAT}(S_{\text{gen}}, S_{\text{ref}}) = \frac{1}{|S_{\text{ref}}|} \sum_{\mathcal{C} \in S_{\text{ref}}} \min_{\hat{\mathcal{C}} \in S_{\text{gen}}} \text{D-MAE}(\mathcal{C}, \hat{\mathcal{C}}), \quad (9)$$

where S_{gen} and S_{ref} denote the sets of generated and reference geometries, respectively, and $|\cdot|$ means the number of elements in a given set. Note that the number of the reference geometry for each reaction is one, which means $|S_{\text{ref}}| = 1$ in our evaluations.

4.4 Computational details

All quantum chemical calculations in this study were performed with Orca [79] at the ω B97X-D3/def2-TZVP level of theory, the same as in Grambow's database [54]. The saddle point optimization was performed using the Berny algorithm [25], and the detailed options are as follows. The Hessian was computed in the first optimization step only. The convergence criteria for the gradients, displacements, and energies were set to 3e-4, 4e-3, and 5e-6 in atomic units, respectively.

To validate multiple TS conformations generated by TSDiff, the single imaginary frequency lower than -100 cm^{-1} was verified, which is the same as in Grambow et al. [54], and the IRC calculation was performed. The maximum iterations of both forward and reverse IRCs were set to 200, and the convergence criterion for the gradients was set to 2e-3 in the atomic unit. After convergence, to ensure that the resulting reactant and product geometries matched those of the reference, we checked the consistency of their molecular connectivity using Open Babel [80].

Data availability. The organic gas-phase reaction database used in this study is available at <https://doi.org/10.1038/s41597-020-0460-4>.

Code availability. The source code of TSDiff will be released upon publication.

Acknowledgments. This work was supported by Korea Environmental Industry and Technology Institute (Grant No. RS202300219144), the National Research Foundation of Korea funded by the Ministry of Science and ICT (Grant No. 2018R1A5A1025208).

Author information. These authors contributed equally: Seonghwan Kim, Jeheon Woo.

References

- [1] Gudiyella, S., Buras, Z.J., Chu, T.-C., Lengyel, I., Pannala, S., Green, W.H.: Modeling study of high temperature pyrolysis of natural gas. *Industrial & Engineering Chemistry Research* **57**(22), 7404–7420 (2018). <https://doi.org/10.1021/acs.iecr.8b00758>
- [2] Gao, C.W., Allen, J.W., Green, W.H., West, R.H.: Reaction mechanism generator: Automatic construction of chemical kinetic mechanisms. *Computer Physics Communications* **203**, 212–225 (2016). <https://doi.org/10.1016/j.cpc.2016.02.013>
- [3] Harper, M.R., Geem, K.M.V., Pyl, S.P., Marin, G.B., Green, W.H.: Comprehensive reaction mechanism for n-butanol pyrolysis and combustion. *Combustion and Flame* **158**(1), 16–41 (2011). <https://doi.org/10.1016/j.combustflame.2010.06.002>
- [4] Bao, J.L., Meana-Pañeda, R., Truhlar, D.G.: Multi-path variational transition state theory for chiral molecules: the site-dependent kinetics for abstraction of hydrogen from 2-butanol by hydroperoxyl radical, analysis of hydrogen bonding in the transition state, and dramatic temperature dependence of the activation energy. *Chemical Science* **6**(10), 5866–5881 (2015). <https://doi.org/10.1039/c5sc01848j>
- [5] Ismail, I., Robertson, C., Habershon, S.: Successes and challenges in using machine-learned activation energies in kinetic simulations. *The Journal of Chemical Physics* **157**(1), 014109 (2022). <https://doi.org/10.1063/5.0096027>
- [6] Park, S., Han, H., Kim, H., Choi, S.: Machine learning applications for chemical reactions. *Chemistry – An Asian Journal* **17**(14) (2022). <https://doi.org/10.1002/asia.202200203>
- [7] Kim, Y., Etz, B.D., Fioroni, G.M., Hays, C.K., John, P.C.S., Messerly, R.A., Vyas, S., Beekley, B.P., Guo, F., McEnally, C.S., Pfefferle, L.D., McCormick, R.L., Kim, S.: Investigation of structural effects of aromatic compounds on sooting tendency with mechanistic insight into ethylphenol isomers. *Proceedings of the Combustion Institute* **38**(1), 1143–1151 (2021). <https://doi.org/10.1016/j.proci.2020.06.321>
- [8] Kim, J.W., Kim, Y., Baek, K.Y., Lee, K., Kim, W.Y.: Performance of ACE-reaction on 26 organic reactions for fully automated reaction network construction and microkinetic analysis. *The Journal of Physical Chemistry A* **123**(22), 4796–4805 (2019). <https://doi.org/10.1021/acs.jpca.9b02161>

- [9] Lee, J.-u., Kim, Y., Kim, W.Y., Oh, H.B.: Graph theory-based reaction pathway searches and DFT calculations for the mechanism studies of free radical-initiated peptide sequencing mass spectrometry (FRIPS MS): a model gas-phase reaction of GGR tri-peptide. *Physical Chemistry Chemical Physics* **22**(9), 5057–5069 (2020). <https://doi.org/10.1039/c9cp05433b>
- [10] Pearson, J.K., Boyd, R.J.: Density functional theory study of the reaction mechanism and energetics of the reduction of hydrogen peroxide by ebselen, ebselen diselenide, and ebselen selenol. *The Journal of Physical Chemistry A* **111**(16), 3152–3160 (2007). <https://doi.org/10.1021/jp071499n>
- [11] Pearson, J.K., Boyd, R.J.: Modeling the reduction of hydrogen peroxide by glutathione peroxidase mimics. *The Journal of Physical Chemistry A* **110**(28), 8979–8985 (2006). <https://doi.org/10.1021/jp0615196>
- [12] Sobez, J.-G., Reiher, M.: MOLASSEMBLER: Molecular graph construction, modification, and conformer generation for inorganic and organic molecules. *Journal of Chemical Information and Modeling* **60**(8), 3884–3900 (2020). <https://doi.org/10.1021/acs.jcim.0c00503>
- [13] Simm, G.N., Vaucher, A.C., Reiher, M.: Exploration of reaction pathways and chemical transformation networks. *The Journal of Physical Chemistry A* **123**(2), 385–399 (2018). <https://doi.org/10.1021/acs.jpca.8b10007>
- [14] Unsleber, J.P., Reiher, M.: The exploration of chemical reaction networks. *Annual Review of Physical Chemistry* **71**(1), 121–142 (2020). <https://doi.org/10.1146/annurev-physchem-071119-040123>
- [15] Simm, G.N., Reiher, M.: Context-driven exploration of complex chemical reaction networks. *Journal of Chemical Theory and Computation* **13**(12), 6108–6119 (2017). <https://doi.org/10.1021/acs.jctc.7b00945>
- [16] Keil, F.: Multiscale modelling in computational heterogeneous catalysis. *Multiscale Molecular Methods in Applied Chemistry*, 69–107 (2012)
- [17] Yang, Z., Gao, W.: Applications of machine learning in alloy catalysts: Rational selection and future development of descriptors. *Advanced Science* **9**(12), 2106043 (2022). <https://doi.org/10.1002/advs.202106043>
- [18] Wang, P., Jin, Z., Li, P., Yu, G.: Design principles of hydrogen-evolution-suppressing single-atom catalysts for aqueous electrosynthesis. *Chem Catalysis* **2**(6), 1277–1287 (2022). <https://doi.org/10.1016/j.checat.2022.04.020>
- [19] Bell, A.T., Head-Gordon, M.: Quantum mechanical modeling of

- catalytic processes. *Annual Review of Chemical and Biomolecular Engineering* **2**(1), 453–477 (2011). <https://doi.org/10.1146/annurev-chembioeng-061010-114108>
- [20] Ziegler, T.: Approximate density functional theory as a practical tool in molecular energetics and dynamics. *Chemical Reviews* **91**(5), 651–667 (1991)
- [21] Kohn, W., Becke, A.D., Parr, R.G.: Density functional theory of electronic structure. *The Journal of Physical Chemistry* **100**(31), 12974–12980 (1996). <https://doi.org/10.1021/jp960669l>
- [22] Zhao, Y., Truhlar, D.G.: Benchmark databases for nonbonded interactions and their use to test density functional theory. *Journal of Chemical Theory and Computation* **1**(3), 415–432 (2005). <https://doi.org/10.1021/ct049851d>
- [23] Cramer, C.J., Truhlar, D.G.: Density functional theory for transition metals and transition metal chemistry. *Physical Chemistry Chemical Physics* **11**(46), 10757 (2009). <https://doi.org/10.1039/b907148b>
- [24] Zimmerman, P.M.: Single-ended transition state finding with the growing string method. *Journal of Computational Chemistry* **36**(9), 601–611 (2015). <https://doi.org/10.1002/jcc.23833>
- [25] Schlegel, H.B.: Optimization of equilibrium geometries and transition structures. *Journal of Computational Chemistry* **3**(2), 214–218 (1982). <https://doi.org/10.1002/jcc.540030212>
- [26] Schlegel, H.B.: Geometry optimization. *WIREs Computational Molecular Science* **1**(5), 790–809 (2011). <https://doi.org/10.1002/wcms.34>
- [27] Lynch, B.J., Truhlar, D.G.: How well can hybrid density functional methods predict transition state geometries and barrier heights? *The Journal of Physical Chemistry A* **105**(13), 2936–2941 (2001). <https://doi.org/10.1021/jp004262z>
- [28] Henkelman, G., Jónsson, H.: Improved tangent estimate in the nudged elastic band method for finding minimum energy paths and saddle points. *The Journal of Chemical Physics* **113**(22), 9978–9985 (2000). <https://doi.org/10.1063/1.1323224>
- [29] Henkelman, G., Uberuaga, B.P., Jónsson, H.: A climbing image nudged elastic band method for finding saddle points and minimum energy paths. *The Journal of Chemical Physics* **113**(22), 9901–9904 (2000). <https://doi.org/10.1063/1.1329672>

- [30] Liu, Y., Qi, H., Lei, M.: Elastic image pair method for finding transition states on potential energy surfaces using only first derivatives. *Journal of Chemical Theory and Computation* **18**(8), 5108–5115 (2022). <https://doi.org/10.1021/acs.jctc.2c00137>
- [31] Suleimanov, Y.V., Green, W.H.: Automated discovery of elementary chemical reaction steps using freezing string and beryny optimization methods. *Journal of Chemical Theory and Computation* **11**(9), 4248–4259 (2015). <https://doi.org/10.1021/acs.jctc.5b00407>
- [32] Zimmerman, P.M.: Growing string method with interpolation and optimization in internal coordinates: Method and examples. *The Journal of Chemical Physics* **138**(18), 184102 (2013). <https://doi.org/10.1063/1.4804162>
- [33] Zimmerman, P.: Reliable transition state searches integrated with the growing string method. *Journal of Chemical Theory and Computation* **9**(7), 3043–3050 (2013). <https://doi.org/10.1021/ct400319w>
- [34] Peters, B., Heyden, A., Bell, A.T., Chakraborty, A.: A growing string method for determining transition states: Comparison to the nudged elastic band and string methods. *The Journal of Chemical Physics* **120**(17), 7877–7886 (2004). <https://doi.org/10.1063/1.1691018>
- [35] Vaucher, A.C., Reiher, M.: Minimum energy paths and transition states by curve optimization. *Journal of Chemical Theory and Computation* **14**(6), 3091–3099 (2018). <https://doi.org/10.1021/acs.jctc.8b00169>
- [36] Maeda, S., Morokuma, K.: Finding reaction pathways of type $A + B \rightarrow X$: Toward systematic prediction of reaction mechanisms. *Journal of Chemical Theory and Computation* **7**(8), 2335–2345 (2011) <https://doi.org/10.1021/ct200290m>. <https://doi.org/10.1021/ct200290m>. PMID: 26606607
- [37] Luo, Y., Maeda, S., Ohno, K.: Automated exploration of stable isomers of $H^+(H_2O)_n$ ($n = 5-7$) via ab initio calculations: An application of the anharmonic downward distortion following algorithm. *Journal of Computational Chemistry* **30**(6), 952–961 (2009) <https://onlinelibrary.wiley.com/doi/pdf/10.1002/jcc.21117>. <https://doi.org/10.1002/jcc.21117>
- [38] Choi, S., Kim, Y., Kim, J.W., Kim, Z., Kim, W.Y.: Feasibility of activation energy prediction of gas-phase reactions by machine learning. *Chemistry - A European Journal* **24**(47), 12354–12358 (2018). <https://doi.org/10.1002/chem.201800345>

- [39] Spiekermann, K.A., Pattanaik, L., Green, W.H.: Fast predictions of reaction barrier heights: Toward coupled-cluster accuracy. *The Journal of Physical Chemistry A* **126**(25), 3976–3986 (2022). <https://doi.org/10.1021/acs.jpca.2c02614>
- [40] Heinen, S., von Rudorff, G.F., von Lilienfeld, O.A.: Toward the design of chemical reactions: Machine learning barriers of competing mechanisms in reactant space. *The Journal of Chemical Physics* **155**(6), 064105 (2021). <https://doi.org/10.1063/5.0059742>
- [41] García-Andrade, X., Tahoces, P.G., Pérez-Ríos, J., Núñez, E.M.: Barrier height prediction by machine learning correction of semiempirical calculations. *The Journal of Physical Chemistry A* **127**(10), 2274–2283 (2023). <https://doi.org/10.1021/acs.jpca.2c08340>
- [42] Marques, E., de Gendt, S., Pourtois, G., van Setten, M.J.: Improving accuracy and transferability of machine learning chemical activation energies by adding electronic structure information. *Journal of Chemical Information and Modeling* **63**(5), 1454–1461 (2023). <https://doi.org/10.1021/acs.jcim.2c01502>
- [43] Lewis-Atwell, T., Townsend, P.A., Grayson, M.N.: Machine learning activation energies of chemical reactions. *WIREs Computational Molecular Science* **12**(4) (2021). <https://doi.org/10.1002/wcms.1593>
- [44] Grambow, C.A., Pattanaik, L., Green, W.H.: Deep learning of activation energies. *The Journal of Physical Chemistry Letters* **11**(8), 2992–2997 (2020). <https://doi.org/10.1021/acs.jpcllett.0c00500>
- [45] Takahashi, K., Miyazato, I.: Rapid estimation of activation energy in heterogeneous catalytic reactions via machine learning. *Journal of Computational Chemistry* **39**(28), 2405–2408 (2018). <https://doi.org/10.1002/jcc.25567>
- [46] Stuyver, T., Coley, C.W.: Quantum chemistry-augmented neural networks for reactivity prediction: Performance, generalizability, and explainability. *The Journal of Chemical Physics* **156**(8), 084104 (2022). <https://doi.org/10.1063/5.0079574>
- [47] Singh, A.R., Rohr, B.A., Gauthier, J.A., Nørskov, J.K.: Predicting chemical reaction barriers with a machine learning model. *Catalysis Letters* **149**(9), 2347–2354 (2019). <https://doi.org/10.1007/s10562-019-02705-x>
- [48] Bragato, M., von Rudorff, G.F., von Lilienfeld, O.A.: Data enhanced hammett-equation: reaction barriers in chemical space. *Chemical Science* **11**(43), 11859–11868 (2020). <https://doi.org/10.1039/d0sc04235h>

- [49] Jackson, R., Zhang, W., Pearson, J.: TSNet: predicting transition state structures with tensor field networks and transfer learning. *Chemical Science* **12**(29), 10022–10040 (2021). <https://doi.org/10.1039/d1sc01206a>
- [50] Makoś, M.Z., Verma, N., Larson, E.C., Freindorf, M., Kraka, E.: Generative adversarial networks for transition state geometry prediction. *The Journal of Chemical Physics* **155**(2), 024116 (2021). <https://doi.org/10.1063/5.0055094>
- [51] Pattanaik, L., Ingraham, J.B., Grambow, C.A., Green, W.H.: Generating transition states of isomerization reactions with deep learning. *Physical Chemistry Chemical Physics* **22**(41), 23618–23626 (2020). <https://doi.org/10.1039/d0cp04670a>
- [52] Choi, S.: Prediction of transition state structures of gas-phase chemical reactions via machine learning. *Nature Communications* **14**(1) (2023). <https://doi.org/10.1038/s41467-023-36823-3>
- [53] Lemm, D., von Rudorff, G.F., von Lilienfeld, O.A.: Machine learning based energy-free structure predictions of molecules, transition states, and solids. *Nature Communications* **12**(1) (2021). <https://doi.org/10.1038/s41467-021-24525-7>
- [54] Grambow, C.A., Pattanaik, L., Green, W.H.: Reactants, products, and transition states of elementary chemical reactions based on quantum chemistry. *Scientific Data* **7**(1) (2020). <https://doi.org/10.1038/s41597-020-0460-4>
- [55] Robertson, C., Habershon, S.: Simple position and orientation preconditioning scheme for minimum energy path calculations. *Journal of Computational Chemistry* **42**(11), 761–770 (2021). <https://doi.org/10.1002/jcc.26495>
- [56] Ramos-Sánchez, P., Harvey, J.N., Gámez, J.A.: An automated method for graph-based chemical space exploration and transition state finding. *Journal of Computational Chemistry* **44**(1), 27–42 (2022). <https://doi.org/10.1002/jcc.27011>
- [57] Kim, H., Woo, J., Kim, S., Moon, S., Kim, J.H., Kim, W.Y.: Predicting quantum chemical property with easy-to-obtain geometry via positional denoising. *arXiv* (2023). <https://doi.org/10.48550/ARXIV.2304.03724>. <https://arxiv.org/abs/2304.03724>
- [58] Godwin, J., Schaarschmidt, M., Gaunt, A., Sanchez-Gonzalez, A., Rubanova, Y., Veličković, P., Kirkpatrick, J., Battaglia, P.: Simple GNN Regularisation for 3D Molecular Property Prediction & Beyond. *arXiv* (2021). <https://doi.org/10.48550/ARXIV.2106.07971>. <https://arxiv.org/>

[abs/2106.07971](https://arxiv.org/abs/2106.07971)

- [59] Ismail, I., Majerus, R.C., Habershon, S.: Graph-driven reaction discovery: Progress, challenges, and future opportunities. *The Journal of Physical Chemistry A* **126**(40), 7051–7069 (2022). <https://doi.org/10.1021/acs.jpca.2c06408>
- [60] Zhao, Q., Hsu, H.-H., Savoie, B.M.: Conformational sampling for transition state searches on a computational budget. *Journal of Chemical Theory and Computation* **18**(5), 3006–3016 (2022). <https://doi.org/10.1021/acs.jctc.2c00081>
- [61] Zhao, Q., Vaddadi, S.M., Woulfe, M., Ogunfowora, L.A., Garimella, S.S., Isayev, O., Savoie, B.M.: Comprehensive exploration of graphically defined reaction spaces. *Scientific Data* **10**(1) (2023). <https://doi.org/10.1038/s41597-023-02043-z>
- [62] Husch, T., Seebach, D., Beck, A.K., Reiher, M.: Rigorous conformational analysis of pyrrolidine enamines with relevance to organocatalysis. *Helvetica Chimica Acta* **100**(10), 1700182 (2017). <https://doi.org/10.1002/hlca.201700182>
- [63] Xu, M., Yu, L., Song, Y., Shi, C., Ermon, S., Tang, J.: GeoDiff: a Geometric Diffusion Model for Molecular Conformation Generation. arXiv (2022). <https://doi.org/10.48550/ARXIV.2203.02923>. <https://arxiv.org/abs/2203.02923>
- [64] Jing, B., Corso, G., Chang, J., Barzilay, R., Jaakkola, T.: Torsional Diffusion for Molecular Conformer Generation. arXiv (2022). <https://doi.org/10.48550/ARXIV.2206.01729>. <https://arxiv.org/abs/2206.01729>
- [65] Hoogeboom, E., Satorras, V.G., Vignac, C., Welling, M.: Equivariant diffusion for molecule generation in 3D. In: *Proceedings of the 39th International Conference on Machine Learning*, vol. 162, pp. 8867–8887. PMLR, Baltimore, Maryland, USA (2022)
- [66] Fukui, K.: The path of chemical reactions - the IRC approach. *Accounts of Chemical Research* **14**(12), 363–368 (1981). <https://doi.org/10.1021/ar00072a001>
- [67] Schrödinger, LLC: The PyMOL Molecular Graphics System, Version 2.0 (2017)
- [68] Daylight Chemical Information Systems, I.: SMARTS - A Language for Describing Molecular Patterns. <http://www.daylight.com/dayhtml/doc/theory/theory.smarts.html> (Accessed on March 29, 2023)

- [69] Welling, M., Teh, Y.W.: Bayesian learning via stochastic gradient langevin dynamics. In: Proceedings of the 28th International Conference on International Conference on Machine Learning. ICML'11, pp. 681–688. Omnipress, Madison, WI, USA (2011)
- [70] Heid, E., Green, W.H.: Machine learning of reaction properties via learned representations of the condensed graph of reaction. *Journal of Chemical Information and Modeling* **62**(9), 2101–2110 (2021). <https://doi.org/10.1021/acs.jcim.1c00975>
- [71] Weininger, D.: Smiles, a chemical language and information system. 1. introduction to methodology and encoding rules. *Journal of chemical information and computer sciences* **28**(1), 31–36 (1988). <https://doi.org/10.1021/ci00057a005>
- [72] Schütt, K.T., Sauceda, H.E., Kindermans, P.-J., Tkatchenko, A., Müller, K.-R.: SchNet – a deep learning architecture for molecules and materials. *The Journal of Chemical Physics* **148**(24), 241722 (2018). <https://doi.org/10.1063/1.5019779>
- [73] Maaten, L.v.d., Hinton, G.: Visualizing data using t-sne. *Journal of Machine Learning Research* **9**, 2579–2605 (2008)
- [74] Pedregosa, F., Varoquaux, G., Gramfort, A., Michel, V., Thirion, B., Grisel, O., Blondel, M., Prettenhofer, P., Weiss, R., Dubourg, V., Vanderplas, J., Passos, A., Cournapeau, D., Brucher, M., Perrot, M., Duchesnay, E.: Scikit-learn: Machine learning in python. *Journal of Machine Learning Research* **12**, 2825–2830 (2011)
- [75] Ho, J., Jain, A., Abbeel, P.: Denoising Diffusion Probabilistic Models. *arXiv* (2020). <https://doi.org/10.48550/ARXIV.2006.11239>. <https://arxiv.org/abs/2006.11239>
- [76] Song, Y., Sohl-Dickstein, J., Kingma, D.P., Kumar, A., Ermon, S., Poole, B.: Score-Based Generative Modeling through Stochastic Differential Equations. *arXiv* (2020). <https://doi.org/10.48550/ARXIV.2011.13456>. <https://arxiv.org/abs/2011.13456>
- [77] Nichol, A., Dhariwal, P.: Improved Denoising Diffusion Probabilistic Models. *arXiv* (2021). <https://doi.org/10.48550/ARXIV.2102.09672>. <https://arxiv.org/abs/2102.09672>
- [78] Ruddigkeit, L., van Deursen, R., Blum, L.C., Reymond, J.-L.: Enumeration of 166 billion organic small molecules in the chemical universe database GDB-17. *Journal of Chemical Information and Modeling* **52**(11), 2864–2875 (2012). <https://doi.org/10.1021/ci300415d>

- [79] Neese, F., Wennmohs, F., Becker, U., Riplinger, C.: The ORCA quantum chemistry program package. *The Journal of Chemical Physics* **152**(22), 224108 (2020). <https://doi.org/10.1063/5.0004608>
- [80] O'Boyle, N.M., Banck, M., James, C.A., Morley, C., Vandermeersch, T., Hutchison, G.R.: Open babel: An open chemical toolbox. *Journal of Cheminformatics* **3**(1) (2011). <https://doi.org/10.1186/1758-2946-3-33>